

1  
2  
3  
4  
5  
6  
7 **Nonlinear regulation of commitment to apoptosis by simultaneous**  
8 **inhibition of Bcl-2 and XIAP in leukemia and lymphoma cells**  
9

10  
11  
12  
13  
14  
15  
16  
17  
18  
19  
20  
21  
22  
23  
24  
25  
26  
27  
28  
29  
30  
31  
32  
33  
34  
35  
36  
37  
38  
39  
40  
41  
42  
43  
44  
45  
46  
47  
48  
49  
50  
51  
52  
53  
54  
55  
56  
57  
58  
59  
60  
61  
62  
63  
64  
65  
Joanna Skommer<sup>1</sup>, Somkanya C Das<sup>2§</sup>, Arjun Nair<sup>2§</sup>, Thomas Brittain<sup>1</sup>, Subhadip Raychaudhuri<sup>2</sup>

<sup>1</sup> School of Biological Sciences, University of Auckland, 3a Symonds Street,

Auckland 1142, New Zealand

<sup>2</sup> Department of Biomedical Engineering, University of California, Davis 95616, USA

§ These authors contributed equally

Correspondence:

J. Skommer, E-mail: [J.Skommer@auckland.ac.nz](mailto:J.Skommer@auckland.ac.nz)

S. Raychaudhuri, E-mail: [raychaudhuri@ucdavis.edu](mailto:raychaudhuri@ucdavis.edu)

1           **Abstract**  
2  
3

4           Background: Apoptosis is a complex pathway regulated by the concerted action of  
5           multiple pro- and anti-apoptotic molecules. The intrinsic (mitochondrial) pathway of  
6           apoptosis is governed up-stream of mitochondria, by the family of Bcl-2 proteins, and  
7           down-stream of mitochondria, by low-probability events, such as apoptosome  
8           formation, and by feedback circuits involving caspases and inhibitor of apoptosis  
9           proteins (IAPs), such as XIAP. All these regulatory mechanisms ensure that cells only  
10          commit to death once a threshold of damage has been reached and the anti-apoptotic  
11          reserve of the cell is overcome. As cancer cells are invariably exposed to strong  
12          intracellular and extracellular stress stimuli, they are particularly reliant on the  
13          expression of anti-apoptotic proteins. Hence, many cancer cells undergo apoptosis  
14          when exposed to agents that inhibit anti-apoptotic Bcl-2 molecules, such as BH3  
15          mimetics, while normal cells remain relatively insensitive to single agent treatments  
16          with the same class of molecules. Targeting different proteins within the apoptotic  
17          network with combinatorial treatment approaches often achieves even greater  
18          specificity.  
19  
20  
21  
22  
23  
24  
25  
26  
27  
28  
29  
30

31  
32          Findings: This led us to investigate the sensitivity of leukemia and lymphoma cells to  
33          a pro-apoptotic action of a BH3 mimetic combined with a small molecule inhibitor of  
34          XIAP. Using computational probabilistic model of apoptotic pathway, verified by  
35          experimental results from human leukemia and lymphoma cell lines, we show that  
36          inhibition of XIAP has a non-linear effect on sensitization towards apoptosis induced  
37          by the BH3 mimetic HA14-1.  
38  
39  
40  
41  
42  
43  
44

45          Conclusions: This study justifies further *ex vivo* and animal studies on the potential of  
46          the treatment of leukemia and lymphoma with a combination of BH3 mimetics and  
47          XIAP inhibitors.  
48  
49  
50  
51  
52  
53  
54  
55  
56  
57  
58  
59  
60  
61  
62  
63  
64  
65

## Introduction

Oncogenic events, such as genomic instability or oncogene activation, can activate BH3-only proteins and induce the mitochondrial pathway of apoptosis [1]. To counteract these death signals, cancer cells often increase the levels of anti-apoptotic Bcl-2 proteins, and become dependent on them [1]. In such cells agents that mimic the Bcl-2 homology 3 (BH3) domains of the pro-apoptotic Bcl-2 family proteins (BH3 mimetics) induce apoptosis in a single-agent treatment scenario [1]. BH3 mimetics bind in a competitive manner to surface hydrophobic grooves of anti-apoptotic Bcl-2 members thereby releasing the pro-apoptotic Bax/Bak molecules otherwise sequestered in complexes with the anti-apoptotic members [1-3]. Once the threshold of activation of Bax/Bak proteins is reached, the mitochondrial outer membrane becomes permeabilized, leading to the release of cytochrome *c* and other pro-apoptotic proteins into the cytosol. This initiates the assembly of the apoptosome, activation of caspase 9, and then activation of the executioner caspases, such as caspase 3 or 7, which not only directly degrade the proteome and commit cells to death, but also provide feedback cleavage of caspase 9. Inhibitor of apoptosis proteins (IAPs), of which XIAP has been the most widely studied, provide an additional level of regulation, as they inhibit consecutive intermediates (caspase 9 and 3/7) in the apoptotic cascade. Upon release from mitochondria, proteins such as Smac/DIABLO bind to XIAP and free the caspases from inhibition, making another contribution to the activation of effector caspases [4].

Targeted small molecules have a promising future in cancer treatment, as they are potent and highly selective for malignant cells. Nevertheless, high doses of BH3 mimetics have been shown to induce cell death also in normal lymphocytes, narrowing their therapeutic window [5, 6]. The combinatorial treatment with synergistic drugs often achieves greater specificity [7], which led us to investigate the sensitivity of leukemia and lymphoma cells to the pro-apoptotic action of a BH3 mimetic combined with a small molecule inhibitor of XIAP [8].

## Materials and methods

### Computational modeling

We developed and studied a Monte Carlo model of the mitochondrial pathway of apoptosis based on our earlier modeling of the same pathway (described in detail in [9,10]). In this stochastic approach we sample diffusion and reaction events of signaling molecules, pertinent to the mitochondrial pathway, using pre-assigned probability constants. Such probabilistic rate constants are directly estimated from experimentally measured diffusion and kinetic rate constants. Proteins with similar functions are simulated in the model by a single representative protein molecule; for example, Bcl-2 represents all functionally similar anti-apoptotic Bcl-2 like inhibitors. BH3 mimetic such as HA14-1 and XIAP inhibitor embelin are integrated in the current simulation scheme in such a manner that large number (or concentration) of molecules can be modeled. The advantage of our stochastic simulation approach is that we can study the impact of both cellular variations in protein levels and inherent stochastic fluctuations in signaling reactions [9,10].

### Cell culture and treatments

Jurkat T, U937, THP-1 $\alpha$ , CEM and Raji cell lines (ACCT) were maintained and treated in RPMI media (Invitrogen) supplemented with L-glutamine (Invitrogen), 1% penicillin/streptomycin mix (Invitrogen), HEPES (Invitrogen), and 10% fetal bovine serum (FBS; Gibco) at 37 °C in humidified 95% air, 5% CO<sub>2</sub>. HEK293 cells were cultured in DMEM (Invitrogen), supplemented as above but without the HEPES. Peripheral blood mononuclear cells (PBMCs) were obtained from fresh blood samples of healthy volunteers using standard Ficoll separation. Following isolation, PBMCs were cultured in RPMI media (Invitrogen), supplemented as for other suspension cell lines. Small molecule BH3 mimetic HA14-1 and a small-molecule inhibitor of XIAP (embelin) were procured from Alexis Biochemicals. Both inhibitors were stored in small aliquots and protected from exposure to light. Cells were treated with either of these inhibitors alone, or in combination, using DMSO as a vehicle control.

### Annexin V/7-AAD assay

To assess cell viability, indicated cell lines were plated on 24-well plates at the density of  $0.3 \times 10^6$  cells/ml, and treated as indicated. At the end of the experiment,

1 cells were collected, washed with PBS, and stained for 20 min at RT with Annexin V-  
2 PE (Invitrogen) and 7-AAD (Invitrogen; 1µg/sample) in the Annexin V binding buffer  
3 (Invitrogen). The cells were analyzed immediately on FACS Calibur (BD). Cells were  
4 gated based on forward scatter (FSC) and side scatter (SSC) to exclude cell debris,  
5 and next analyzed based on Annexin V-PE fluorescence and 7-AAD fluorescence  
6 using CellQuest (BD). Plots were generated using WinMDA.  
7  
8  
9  
10

### 11 **Detection of caspase activity**

12 Activation of caspase 9 was examined by a dual labelling of cells with PhiPhiLux-  
13 G<sub>1</sub>D<sub>1</sub> reagent (OncoImmunin Ltd.), which allows real-time detection of caspase 3  
14 activation, and 7-AAD (Invitrogen), a probe of plasma membrane permeability.  
15 Briefly,  $1 \times 10^6$  cells were cultured for the time indicated with or without the  
16 indicated doses of HA14-1 and/or embelin, harvested, and incubated with PhiPhiLux-  
17 G<sub>1</sub>D<sub>1</sub> following the manufacturer's instructions. Next, cells were stained with 7-AAD  
18 for 3 min, and immediately analyzed on a FACS Calibur (BD). Cells were gated  
19 based on forward scatter (FSC) and side scatter (SSC) to exclude cell debris, and  
20 based on FSC versus 7-AAD to exclude cells with plasma membrane permeability.  
21 Plots were generated using WinMDA.  
22  
23  
24  
25  
26  
27  
28  
29  
30  
31  
32  
33  
34  
35  
36

### 37 **Results and Discussion**

38 Using systems level information of the apoptotic signaling reactions (Fig. 1), we have  
39 developed a computational model of the mitochondrial pathway of apoptosis, which  
40 can be applied to study the activation of caspases over a wide range of apoptotic  
41 network parameters (described in detail in [9]). The model explicitly simulates  
42 diffusion and reaction events at the level of individual molecules, and is based on a  
43 probabilistic method in which the reactivity of all the signaling molecules follows a  
44 stochastic, rather than deterministic behavior, probing the induction of apoptosis at a  
45 single cell level [10]. At the beginning of the simulation all signaling molecules are  
46 distributed randomly and uniformly in the cell volume simulated by a three  
47 dimensional cubic lattice. Cytochrome *c* molecules are confined within a fixed  
48 mitochondrial region inside the cell volume. Once the concentration of active Bax  
49 dimers reaches a pre-assigned threshold value ( $\sim 0.017 \mu\text{m}$ ), cytochrome *c* is released  
50  
51  
52  
53  
54  
55  
56  
57  
58  
59  
60  
61  
62  
63  
64  
65

1 from the mitochondria into the cytosol in an all-or-none manner [11]. The proteins  
2 with similar biochemical activities are represented by single species in our  
3 simulations. For example, Bax represents all pro-apoptotic multi-domain Bcl-2  
4 proteins (i.e. both Bax and Bak), whereas Bcl-2 represents all anti-apoptotic Bcl-2  
5 proteins (e.g. Bcl-2, Bcl-X<sub>L</sub>, Mcl-1, etc.). The model uses truncated Bid (tBid),  
6 enhanced by the action of BH3 mimetic HA14-1, as a trigger for the Bax activation in  
7 the mitochondrial pathway of apoptosis. With this approach we have previously  
8 shown that Bcl-2 regulates cell-to-cell variability in time-to-death, and that stochastic  
9 fluctuations in apoptotic reactions are sufficient for survival of single cells upon  
10 treatment with a BH3 mimetic [9]. In single cells, mitochondrial stress is translated  
11 into a binary decision at the level of caspase activation, which is subject to further  
12 regulation by feedback loops, e.g. involving XIAP, caspase 9 and caspase 3 (Fig. 1).  
13 Such a feedback loop can be used to suppress weak post-mitochondrial stress signals,  
14 increasing cell-to-cell variability [12-14]. Increased XIAP expression has been  
15 reported in a variety of human tumors as well as in leukemic cell lines, and XIAP  
16 over-expression (or higher XIAP/Smac ratio) has been linked to poor prognosis  
17 [15,16]. In our computational model a two-fold increase in the average value of  
18 XIAP, from 18 (corresponding to 30nM concentration, as found in normal cells) to 36  
19 (corresponding to 60nM concentration), did not have a significant effect on inhibition  
20 of apoptosis (Fig. 2a). A ten-fold increase in the average XIAP level, however, had a  
21 strong inhibitory effect on cell death activation (Fig. 2a). Ten-fold increase in XIAP  
22 level could also effectively reduce the threshold Bcl-2 level needed to suppress  
23 apoptotic death, a strategy that can be used by cancer cells to overcome their inherent  
24 vulnerability to apoptosis caused by oncogenic activation of pro-apoptotic BH3-only  
25 proteins. Our computational model of apoptosis (tBid mediated) indicated that the  
26 effect of XIAP on inhibition of sensitivity to cell death has a non-linear nature due to  
27 coupling of XIAP to several signalling molecules downstream of mitochondria, which  
28 generates a loop structures (Fig. 1, grey box). When Bcl-2 and XIAP are inhibited by  
29 HA14-1 and embelin, respectively, in a combined treatment, effective induction of  
30 cell death is observed at a lower dose of HA14-1 (Fig. 2b). Further increase in  
31 embelin concentration did not significantly increase apoptotic death induced by  
32 varying doses of HA14-1, again underscoring the non-linear pro-apoptotic effect of  
33 the combinatory treatment (Fig. 2b).

1 To validate the predictions of the mathematical modeling we analyzed the  
2 induction of apoptosis in Jurkat T cells treated with increasing concentrations of the  
3 BH3 mimetic HA14-1 (Axxora), alone or in combination with embelin (Sigma).  
4 Apoptotic cell death was measured using Annexin V and 7-AAD (both from  
5 Invitrogen) and flow cytometry (FACSCalibur, BD) (Fig. 3a). Administration of  
6  
7 embelin significantly enhanced apoptotic cell death induced by HA14-1 (Fig. 3b).  
8  
9 Importantly, while cell death induced by low doses (5-10 $\mu$ M) of HA14-1 increased  
10 significantly upon co-treatment with embelin, this effect was not observed at higher  
11 doses of HA14-1 (Fig. 3b), confirming the nonlinear effect of XIAP inhibition as  
12 suggested by our computational modeling. We also studied cell lines derived from  
13 other hematological malignancies, including monocytic leukemia (THP-1 $\alpha$ ),  
14 histiocytic lymphoma (U937), T-cell acute lymphoblastic leukemia (CEM), and B-cell  
15 lymphoma (RAJI), and observed again that embelin enhances significantly cell death  
16 induced by low doses (5-10 $\mu$ M) of HA14-1 (Fig. S1 and data not shown). Using a  
17 fixed-ratio analysis of the pharmacological interactions between HA14-1 and embelin  
18 we observed that co-administration of the two compounds is synergistic [17] at the  
19 doses of HA14-1 that induce only limited cell death in a single-agent treatment,  
20 independently of the cell line used (Fig. 3c). However, administration of embelin did  
21 not sensitize to cell death induced by higher doses of HA14-1 (Fig. 3c), again  
22 confirming the non-linear effect of XIAP inhibition on sensitivity to the BH3 mimetic.  
23 Importantly, non-cancerous HEK293 cells, which are resistant to cell death induced  
24 by HA14-1 [9], were not sensitized by embelin (3d). Similarly, in peripheral blood  
25 mononuclear cells (PBMCs), obtained from healthy individuals, treatment with  
26 embelin did not enhance HA14-1-induced apoptosis (Fig. 3e).

27  
28  
29 We showed previously that the combined effects of (a) all-or-none activation of  
30 caspase 9 and 3 at the single cell level, and (b) cell-to-cell fluctuations lead to bi-  
31 modal probability distributions for activated caspase 9 and 3 [9]. This study shows  
32 that the combined effect of higher Bcl-2 and XIAP levels leads to efficient  
33 suppression of cell death, and results in an increase in the time-to-death and its cell-to-  
34 cell variability. In a combined HA14-1-embelin treatment scenario, increase in  
35 embelin dose resulted in decreased cell-to-cell variability in time-to-death but the  
36 characteristic all-or-none type activation remained preserved (Fig. 4). Such all-or-  
37 none type activation with cell-to-cell variability leads to bi-modal probability  
38  
39  
40  
41  
42  
43  
44  
45  
46  
47  
48  
49  
50  
51  
52  
53  
54  
55  
56  
57  
58  
59  
60  
61  
62  
63  
64  
65

1 distributions in caspase-3 activation [9,10], which can be used for quantitative  
2 estimation of cell-to-cell variability in apoptosis activation [Fig. 5a]. Direct estimation  
3 of cell-to-cell variability in time-to-death, such as its variance, is problematic because  
4 only a fraction of cells undergoes apoptosis at a given time. Assuming perfect bi-  
5 modal curves, the ratio variance/average for caspase 3 activity is found to be  $C3[1-$   
6  $f(e,t)]$ , where  $C3$  is the initial number of Caspase 3 molecules and  $f(e,t)$  denotes the  
7 fraction of cells in which caspase 3 has undergone complete activation (for a given  
8 embelin concentration  $e$  at time  $t$ ) [9]. Estimation of  $C3[1-f(e,t)]$  from Fig. 4 (at the  
9 end of simulation,  $t = 5 \times 10^4$  seconds):  $0.81C3$  (embelin = 200 molecules,  $\sim 0.33$   
10  $\mu\text{M}$ ),  $0.44C3$  (embelin = 1000 molecules,  $\sim 1.67 \mu\text{M}$ ) and  $0.37C3$  (embelin = 2000  
11 molecules,  $\sim 3.33 \mu\text{M}$ ), which indicates a decrease in cell-to-cell variability due to  
12 increased XIAP inhibition (by increased concentration of embelin). In our  
13 simulations, a cellular average of  $C3 = 60$  molecules ( $\sim 100 \text{ nm}$ ) is used for inactive  
14 caspase 3 molecules. Estimation of variance/average from the experimental data  
15 (early apoptotic cells in Fig. 3b) also shows decreased cell-to-cell variability with  
16 increased XIAP inhibition:  $0.91C3$  (embelin = 0),  $0.83C3$  (embelin =  $10 \mu\text{M}$ ),  
17  $0.66C3$  (embelin =  $20 \mu\text{M}$ ) for HA14-1 =  $5 \mu\text{M}$ .

18  
19  
20  
21  
22  
23  
24  
25  
26  
27  
28  
29  
30  
31  
32 To validate the findings of the computational model, we analyzed the distribution of  
33 caspase 3 activity in early apoptotic cells using caspase 3 recognition sequence  
34 DEVDGI labeled with a fluorophore (PhiPhiLux-G<sub>1</sub>D<sub>1</sub>) and 7-AAD (a marker of  
35 early plasma membrane permeabilisation). Treatment with HA14-1 led to increased  
36 caspase 9 activity, with a clearly distinguishable population of cells with over 10-fold  
37 increase in PhiPhiLux-G<sub>1</sub>D<sub>1</sub> fluorescence (Fig. 5b). The intermediate events in terms  
38 of caspase 3 activity were infrequent ( $<8\%$ ; M2 on Figure 5b), in line with our  
39 previous observations [8]. Upon addition of inhibitor of XIAP embelin there was an  
40 approximately two-fold increase (up to 15%) in the number of intermediate caspase 3  
41 activation events (Fig. 5b). This confirms that direct inhibition of XIAP, and thus  
42 interference in feedback loops that regulate activation of caspases downstream of  
43 mitochondria, can somehow disturb the bimodal distribution of caspase 3 activity.  
44  
45 Considering the possibility of non-specific labeling with reagents such as PhiPhiLux,  
46 which contain an artificial caspase cleavage site, as well as varying sensitivity of  
47 different approaches for detection of caspase activity, it will be of interest to perform  
48 similar analysis using alternative experimental avenues that allow assessment of  
49  
50  
51  
52  
53  
54  
55  
56  
57  
58  
59  
60  
61  
62  
63  
64  
65



1 caspase activity in living cells, for example with the use of recently described crown  
2 nanoparticle probes [18].  
3

4  
5 The advantage of *in silico* models of cellular systems is that one can  
6 selectively study the behavior of specific pathways, reducing the complexity of  
7 biological systems, and thus test concepts that are otherwise difficult to verify  
8 experimentally [10, 19]. Recent developments in the field of computational systems  
9 biology have paved the way to important new discoveries pertinent to cancer therapy  
10 [9, 20, 21]. Mathematical approaches range from models of cancer epidemiology [22]  
11 or models reproducing the dynamics of accumulation of genetic changes during  
12 tumorigenesis [23], through computational tools for predicting response of cancer  
13 cells to treatment [24], up to early stage models for design of patient-specific  
14 immunotherapy [25], and all provide invaluable insights into cancer biology.  
15  
16 Considering the importance of apoptotic cell death in tumorigenesis as well as cancer  
17 therapy, a detailed systems-level understanding of this pathway is also likely to yield  
18 clinically-relevant information. Even though there are some discrepancies between the  
19 behavior of the computational model and the real cellular systems, which may be due  
20 to the off-target effects of the BH3 mimetic *in vitro*, particularly at higher  
21 concentrations, approximate quantitative data for some protein species in the  
22 computational model, or the fact that the combination of tBid and HA14-1 is used in  
23 our model, the general behaviour of our model and biological system follows the  
24 same trend.  
25  
26  
27  
28  
29  
30  
31  
32  
33  
34  
35  
36  
37  
38  
39

40  
41 Our network analysis suggests that once the anti-apoptotic reserve of a cell is  
42 overwhelmed by inhibition of both Bcl-2 and XIAP, a higher sensitivity of cancer  
43 cells to small doses of BH3 mimetics is observed. Our computational model of  
44 apoptosis suggested a nonlinear effect of XIAP inhibition, which we verified  
45 experimentally in several leukemia and lymphoma cell lines. Such non-linear effect of  
46 XIAP, expression of which is regulated by cytokines and other survival factors  
47 through the PI3K/MAPK pathway [16], can provide a mechanism for unusual  
48 apoptosis resistance of cancer cells. Therefore, a combination of low doses of BH3  
49 mimetics with a pharmacological inhibitor of XIAP embelin represents a particularly  
50 promising strategy for the treatment of hematological malignancies. Our  
51 computational studies indicate that combined inhibition of both Bcl-2 and XIAP can  
52  
53  
54  
55  
56  
57  
58  
59  
60  
61  
62  
63  
64  
65

1  
2  
3  
4  
5  
6  
7  
8  
9  
10  
11  
12  
13  
14  
15  
16  
17  
18  
19  
20  
21  
22  
23  
24  
25  
26  
27  
28  
29  
30  
31  
32  
33  
34  
35  
36  
37  
38  
39  
40  
41  
42  
43  
44  
45  
46  
47  
48  
49  
50  
51  
52  
53  
54  
55  
56  
57  
58  
59  
60  
61  
62  
63  
64  
65

reduce cell-to-cell variability in cell death and thus can reduce fractional killing of tumor cells [9]. This study seems to hold sufficient promise to justify further *ex vivo* and animal studies on the potential of the treatment of leukemia and lymphoma with a combination of BH3 mimetics and embelin.

### **Authors' contribution**

JS and TB carried out the experimental studies. SR, SD, and AN designed and carried out the computational studies. JS and SR conceived the study and drafted the manuscript. TB, SD, and AN helped in preparation of the manuscript. All authors read and approved the final manuscript.

### **Acknowledgments**

We are grateful to Prof. R. Dunbar (SBS, University of Auckland) for providing U937 and peripheral blood mononuclear cells, Prof B. Baguley (UoA) for providing Raji CEM and HL-60 cells, Dr J. Taylor (SBS, UoA) for THP-1 $\alpha$  cells, and Dr D. Wlodkowic (Department of Chemistry, UoA) for providing PhiPhiLux-G<sub>1</sub>D<sub>1</sub> reagent.

## References

1. Chonghaile TN, Letai A. Mimicking the BH3 domain to kill cancer cells. *Oncogene* 2008; 27 Suppl 1:S149-57.
2. Labi V, Grespi F, Baumgartner F, Villunger A. Targeting the Bcl-2-regulated apoptosis pathway by BH3 mimetics: a breakthrough in anticancer therapy? *Cell Death Differ.* 2008; 15:977-87.
3. Skommer J, Wlodkowic D, Deptala A. Larger than life: Mitochondria and the Bcl-2 family. *Leuk. Res.* 2007; 31:277-86.
4. Du C, Fang M, Li Y, Li L, Wang X. Smac, a mitochondrial protein that promotes cytochrome *c*-dependent caspase activation by eliminating IAP inhibition. *Cell* 2000; 102:33–42.
5. Kohl TM, Hellinger C, Ahmed F, Buske C, Hiddemann W, Bohlander SK, Spiekermann K. BH3 mimetic ABT-737 neutralizes resistance to FLT3 inhibitor treatment mediated by FLT3-independent expression of BCL2 in primary AML blasts. *Leukemia* 2007; 21:1763-72.
6. High LM, Szymanska B, Wilczynska-Kalak U, Barber N, O'Brien R, Khaw SL, Vikstrom IB, Roberts AW, Lock RB. The Bcl-2 homology domain 3 mimetic ABT-737 targets the apoptotic machinery in acute lymphoblastic leukemia resulting in synergistic in vitro and in vivo interactions with established drugs. *Mol. Pharmacol.* 2010; 77:483-94.
7. Lehár J, Krueger AS, Avery W, Heilbut AM, Johansen LM, Price ER, *et al.* Synergistic drug combinations tend to improve therapeutically relevant selectivity. *Nat. Biotechnol.* 2009; 27:659-66.
8. Nikolovska-Coleska Z, Xu L, Hu Z, Tomita Y, Li P, Roller PP, *et al.* Discovery of embelin as a cell-permeable, small-molecular weight inhibitor of XIAP through structure-based computational screening of a traditional herbal medicine three-dimensional structure database. *J. Med. Chem.* 2004; 47:2430-40.
9. Skommer J, Brittain T, Raychaudhuri S. Bcl-2 inhibits apoptosis by increasing the time-to-death and intrinsic cell-to-cell variations in the mitochondrial pathway of cell death. *Apoptosis* 2010; 15:1223-33.
10. Raychaudhuri S, Willgohe E, Nguyen TN, Khan EM, Goldkorn T. Monte Carlo simulation of cell death signaling predicts large cell-to-cell stochastic

1  
2  
3  
4  
5  
6  
7  
8  
9  
10  
11  
12  
13  
14  
15  
16  
17  
18  
19  
20  
21  
22  
23  
24  
25  
26  
27  
28  
29  
30  
31  
32  
33  
34  
35  
36  
37  
38  
39  
40  
41  
42  
43  
44  
45  
46  
47  
48  
49  
50  
51  
52  
53  
54  
55  
56  
57  
58  
59  
60  
61  
62  
63  
64  
65

fluctuations through the type 2 pathway of apoptosis. *Biophys. J.* 2008;  
95(8):3559-62.

11. Goldstein JC, Waterhouse NJ, Juin P, Evan GI, Green DR. The coordinate release of cytochrome c during apoptosis is rapid, complete and kinetically invariant. *Nat Cell Biol.* 2000; 2:156-62.
12. Albeck JG, Burke JM, Spencer SL, Lauffenburger DA, Sorger PK. Modeling a snap-action, variable-delay switch controlling extrinsic cell death. *PLoS Biol.* 2008; 6:2831-52.
13. Rehm M, Huber HJ, Dussmann H, Prehn JH. Systems analysis of effector caspase activation and its control by X-linked inhibitor of apoptosis protein. *EMBO J.* 2006; 25:4338-49.
14. Legewie S, Blüthgen N, Herzog H. Mathematical modeling identifies inhibitors of apoptosis as mediators of positive feedback and bistability. *PLoS Comput. Biol.* 2006; 2:e120.
15. Tamm I, Kornblau SM, Segall H, Krajewski S, Welsh K, Kitada S, Scudiero DA, Tudor G, Qui YH, Monks A, Andreeff M, Reed JC. Expression and prognostic significance of IAP-family genes in human cancers and myeloid leukemias. *Clin. Cancer. Res.* 2000; 6(5):1796-803.
16. Carter BZ, Milella M, Tsao T, McQueen T, Schober WD, Hu W, Dean NM, Steelman L, McCubrey JA, Andreeff M. Regulation and targeting of antiapoptotic XIAP in acute myeloid leukemia. *Leukemia* 2003; 17(11):2081-9.
17. Dressler V, Müller G, Sühnel J. CombiTool--a new computer program for analyzing combination experiments with biologically active agents. *Comput. Biomed. Res.* 1999; 32:145-60.
18. Jun YW, Sheikholeslami S, Hostetter DR, Tajon C, Craik CS, Alivisatos AP. Continuous imaging of Plasmon rules in live cells reveals early-stage caspase-3 activation at the single-molecule level. *Proc. Natl. Acad. Sci. USA* 2009; 106:17735-40.
19. Raychaudhuri S. Minimal model of a signaling network elucidates cell-to-cell stochastic variability in apoptosis. *PLoS One* 2010; 5:e11930.
20. Swierniak A, Kimmel M, Smieja J. Mathematical modeling as a tool for planning anticancer therapy. *Eur. J. Pharmacol.* 2009; 625(1-3):108-21.

- 1  
2  
3  
4  
5  
6  
7  
8  
9  
10  
11  
12  
13  
14  
15  
16  
17  
18  
19  
20  
21  
22  
23  
24  
25  
26  
27  
28  
29  
30  
31  
32  
33  
34  
35  
36  
37  
38  
39  
40  
41  
42  
43  
44  
45  
46  
47  
48  
49  
50  
51  
52  
53  
54  
55  
56  
57  
58  
59  
60  
61  
62  
63  
64  
65
21. Marin-Sanguino A., Gupta S.K., Voit E.O., Vera J. Biochemical pathway modeling tools for drug target detection in cancer and other complex diseases. *Methods Enzymol.* 2011; 487:319-69.
  22. Liso A, Castiglione F, Cappuccio A, Stracci F, Schlenk RF, Amadori S, Thiede C, Schnittger S, Valk PJ, Döhner K, Martelli MF, Schaich M, Krauter J, Ganser A, Martelli MP, Bolli N, Löwenberg B, Haferlach T, Ehninger G, Mandelli F, Döhner H, Michor F, Falini B. A one-mutation mathematical model can explain the age incidence of acute myeloid leukemia with mutated nucleophosmin (NPM1). *Haematologica.* 2008; 93(8):1219-26.
  23. Attolini CS, Cheng YK, Beroukhim R, Getz G, Abdel-Wahab O, Levine RL, Mellinghoff IK, Michor F. A mathematical framework to determine the temporal sequence of somatic genetic events in cancer. *Proc Natl Acad Sci U S A.* 2010; 107(41):17604-9.
  24. Foo J, Drummond MW, Clarkson B, Holyoake T, Michor F. Eradication of chronic myeloid leukemia stem cells: a novel mathematical model predicts no therapeutic benefit of adding G-CSF to imatinib. *PLoS Comput. Biol.* 2009; 5(9):e1000503.
  25. Kronik N, Kogan Y, Elishmereni M, Halevi-Tobias K, Vuk-Pavlović S, Agur Z. Predicting outcomes of prostate cancer immunotherapy by personalized mathematical models. *PLoS One.* 2010; 5(12):e15482.
  26. Wang JL, Liu D, Zhang ZJ, Shan S, Han X, Srinivasula SM, Croce CM, Alnemri ES, Huang Z. Structure-based discovery of an organic compound that binds Bcl-2 protein and induces apoptosis of tumor cells. *Proc. Natl. Acad. Sci. U S A.* 2000; 97(13):7124-9.

1 **Figure 1** Schematic of the mitochondrial pathway network used in the probabilistic  
2 computational model. MOMP, mitochondrial outer membrane permeabilisation;  
3 XIAP, X-linked inhibitor of apoptosis protein. The model emulates the experimental  
4 set up by using HA14-1 as a stress trigger, and embelin as XIAP inhibitor. Binding  
5 affinity of HA14-1 to Bcl-2 and embelin to XIAP were based on previously published  
6 data (8, 26).  $K_D$ , dissociation constant.  
7  
8  
9

10  
11  
12 **Figure 2** Probabilistic computational model of apoptosis suggests that inhibition of  
13 XIAP leads to a nonlinear increase in sensitivity to apoptosis. Data was obtained after  
14  $5 \times 10^8$  Monte Carlo (MC) simulation steps. 1MC step =  $10^{-4}$  seconds.  
15  
16

17 (A) The percentage of apoptotic cells is shown for various levels of Bcl-2 and XIAP.  
18 We did not observe any activation for Bcl-2 = 2250 (number of molecules) and XIAP  
19 = 180 (number of molecules). XIAP (or Bcl-2) concentration (in nanomolar) was  
20 1.67 times the number of molecules used in our simulations.  
21

22 (B) Increasing apoptotic stress (combined dose of HA14-1 and embelin), with Bcl-2 =  
23 2250 (number of molecules) and XIAP = 180 (number of molecules). Concentration  
24 for a molecular species can be obtained by multiplying the number of molecules with  
25 a factor of 1.67.  
26  
27

28  
29  
30  
31  
32  
33  
34 **Figure 3** Embelin is synergistic with low doses of HA14-1 in leukemia cells, but not  
35 in normal cells  
36

37 (A) Jurkat T cells were treated with increasing concentration of HA14-1, alone or  
38 with embelin, and the percentage of viable, early and late apoptotic cells was  
39 determined by flow cytometry. Cells negative for Annexin V/7-AAD staining (R2)  
40 are considered as viable; Annexin V positive cells are considered as early apoptotic  
41 (R3) or late apoptotic (R4), depending on the permeability to 7-AAD.  
42

43 (B) Data from 3 independent experiments on Jurkat T cells are shown as mean  $\pm$   
44 SEM. <sup>a</sup>  $p < 0.05$  compared to HA14-1 5 $\mu$ M; <sup>b</sup>  $p < 0.05$  compared to HA14-1 10 $\mu$ M  
45

46 (C) Indicated cells were cultured in the presence of escalating doses of HA14-1 (0-  
47 25 $\mu$ M) or embelin (0-70 $\mu$ M), used for the calculation of the theoretical dose-response  
48 surface in combinatory treatments, or combinations of the 2 agents at a 1:2 molar ratio  
49 (5/10, 7.5/15, 10/20, 12.5/25, 15/30, 20/40). The percentage of apoptotic cells was  
50 determined after 24h using flow cytometry. The results were analyzed using the  
51 CombiTool software (9, 18). The experimental data (●) was compared with the  
52  
53  
54  
55  
56  
57  
58  
59  
60  
61  
62  
63  
64  
65

1 theoretical dose–response surface (○) representing the calculated additive effect of  
2 the combined doses of HA14-1 and embelin. If the experimental data points are  
3 mapped above the theoretical surface, coincided with it, or were below it, the  
4 interaction of modalities is defined as synergistic, additive, or antagonistic,  
5 respectively. The computed experimental data is the mean of 3 independent  
6 experiments.  
7  
8  
9

10 (D) HEK293 cells were treated with DMSO or HA14-1 (25μM), with or without  
11 embelin (30μM), and after 24h their viability was analyzed as in a). Data from 3  
12 independent experiments are shown as mean ± SEM.  
13  
14  
15

16 (E) Percentage of apoptotic cells after the indicated treatment of peripheral blood  
17 mononuclear cells from healthy individuals, assessed as in (a). Data from a  
18 representative sample out of 3 analyzed is shown.  
19  
20  
21  
22

23 **Figure 4** Effects of XIAP inhibition on the cell-to-cell variability in caspase  
24 activation.  
25  
26

27 Time course of capsase-3 activation (normalized to 1) is shown as obtained from the  
28 computational model. Time is shown in Monte Carlo (MC) simulation steps up to 5 x  
29 10<sup>8</sup> MC steps (1 MC step = 10<sup>-4</sup> seconds). Three Embelin values (top to bottom) are  
30 used in our simulations: 200, 1000, and 2000 (number of molecules) and HA14-1 =  
31 1800 molecules (concentration ~ 3 μM). Number of molecules of Bcl-2 = 2250 and  
32 XIAP = 180. Data is shown for 15 individual single cell runs (only a fraction of cells  
33 show activation within the given simulation time).  
34  
35  
36  
37  
38  
39  
40  
41

42 **Figure 5** Effects of XIAP inhibition on the bi-stable mode of caspase activation in  
43 HA14-1-treated cells  
44

45 (A) Probability distribution of caspase-3 activation at time steps = 10<sup>4</sup>, 2 x 10<sup>8</sup> and 5 x  
46 10<sup>8</sup> (left to right). Time is shown in Monte Carlo (MC) simulation steps (1 MC step =  
47 10<sup>-4</sup> seconds). Three Embelin values (top to bottom) are used in our simulations: 200,  
48 1000, and 2000 (number of molecules). Number of molecules of Bcl-2 = 2250, XIAP  
49 = 180, and HA141-1 = 1800. Concentration for a molecular species can be obtained  
50 by multiplying the number of molecules with a factor of 1.67. Data is obtained from  
51 16 individual single cell runs.  
52  
53  
54  
55  
56  
57  
58  
59  
60  
61  
62  
63  
64  
65

(B) Jurkat T cells were treated as indicated (embelin 20 $\mu$ M) for 24h, stained with PhiPhiLux-G<sub>1</sub>D<sub>1</sub>, and analyzed by flow cytometry. M1, full caspase activation; M2, intermediate caspase activation; M3, no caspase activation. The population of 7-AAD negative cells was analyzed to exclude for potential loss of caspase labeling during the later stages of cell death.

1  
2  
3  
4  
5  
6  
7  
8  
9  
10  
11  
12  
13  
14  
15  
16  
17  
18  
19  
20  
21  
22  
23  
24  
25  
26  
27  
28  
29  
30  
31  
32  
33  
34  
35  
36  
37  
38  
39  
40  
41  
42  
43  
44  
45  
46  
47  
48  
49  
50  
51  
52  
53  
54  
55  
56  
57  
58  
59  
60  
61  
62  
63  
64  
65



Figure 1

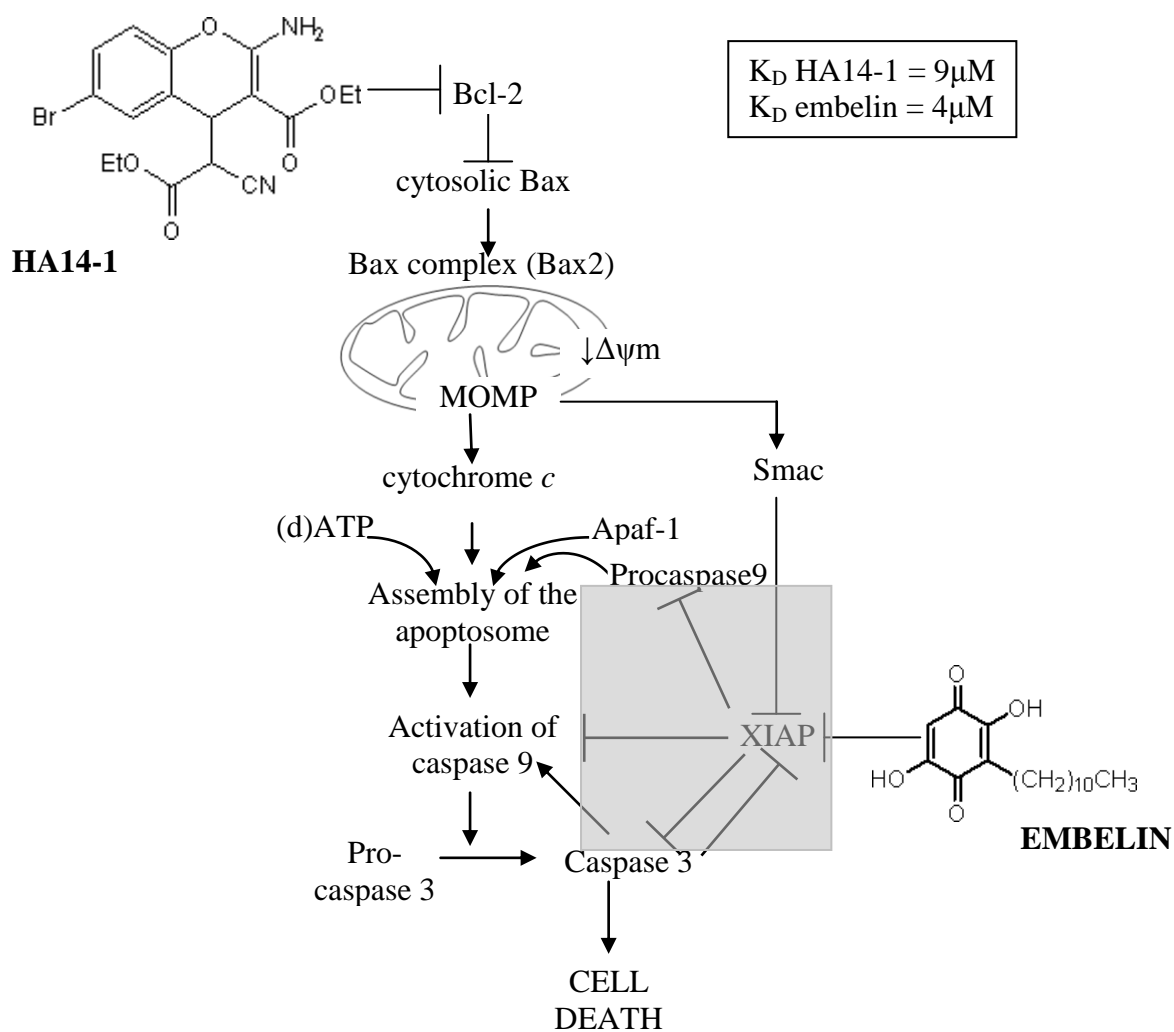


**Figure 2**

[Click here to download Figure: Figure 2A-2B.doc](#)

Figure 2

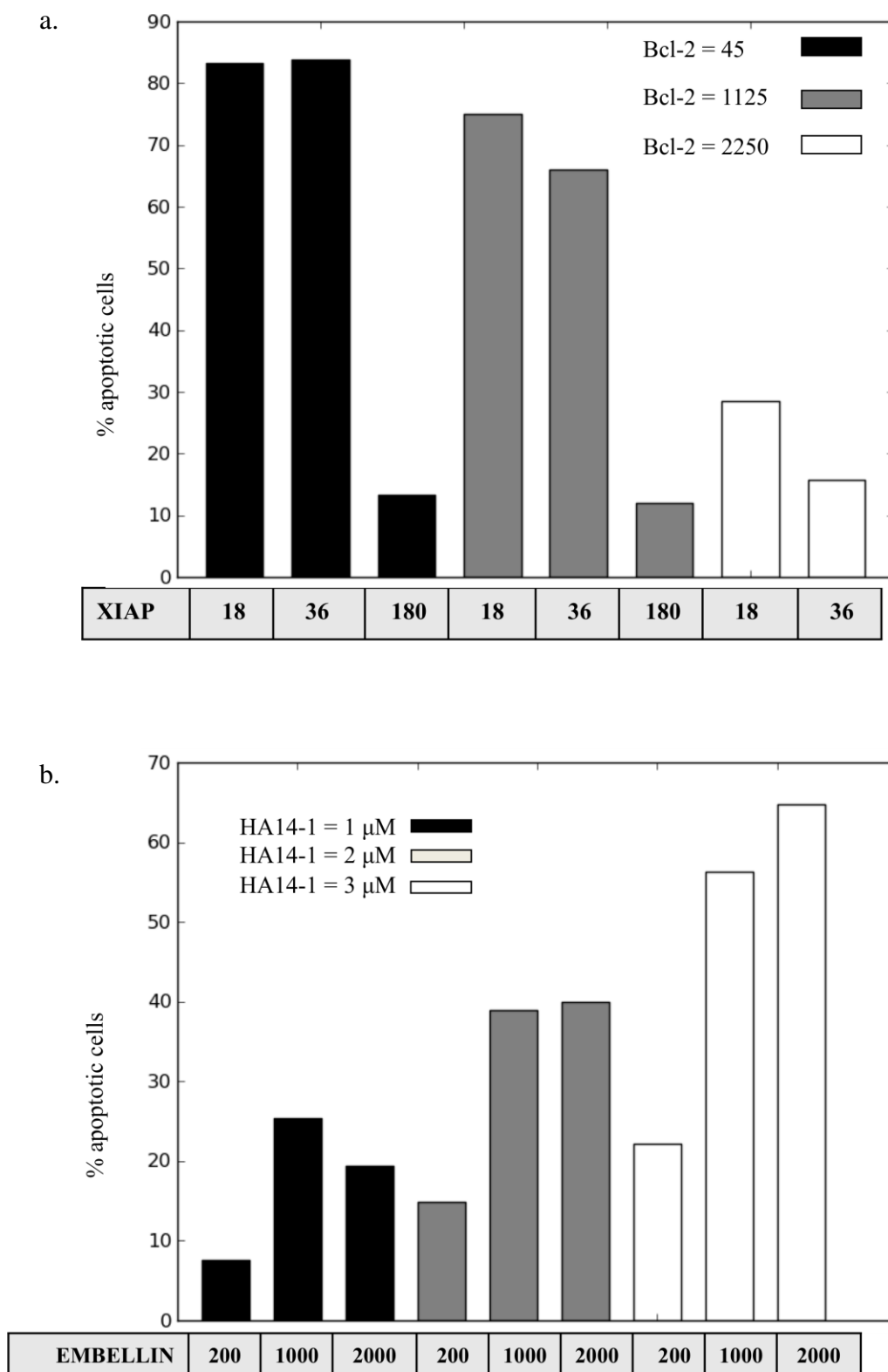
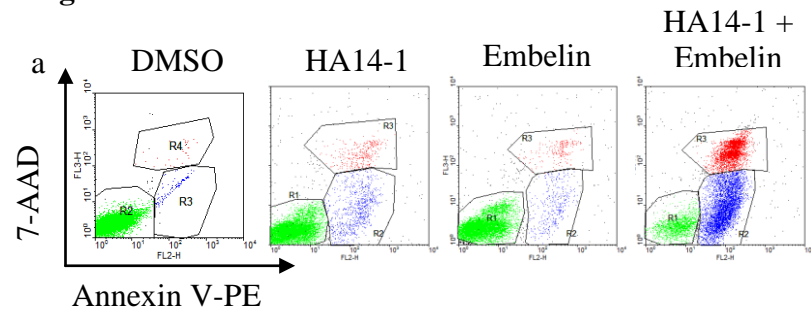


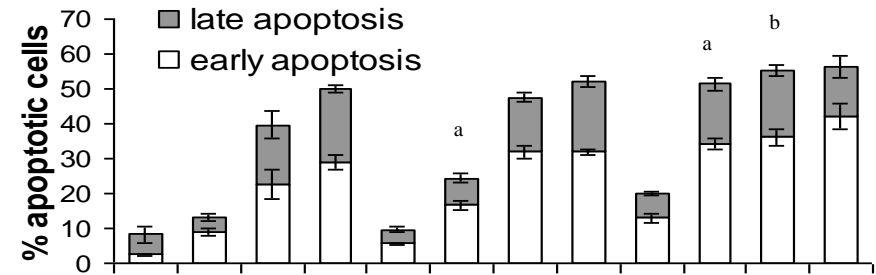
**Figure 3**

[Click here to download Figure: Figure 3.doc](#)

**Figure 3**

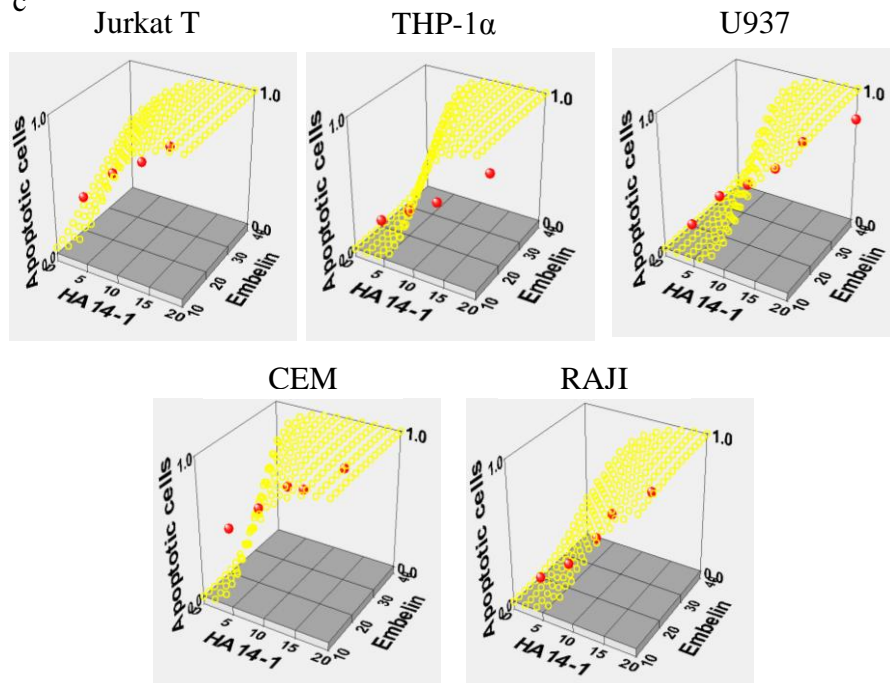


**b**

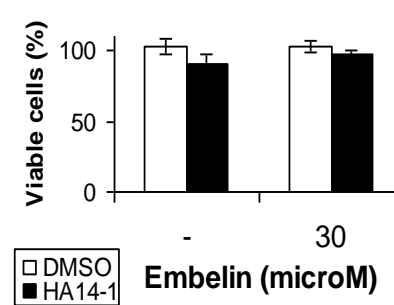


HA14-1 $\mu\text{M}$	-	5	10	12.5	0	5	10	12.5	0	5	10	12.5
Embelin $\mu\text{M}$	-	-	-	-	10	10	10	10	20	20	20	20

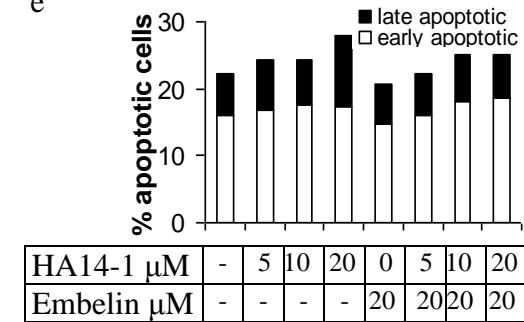
**c**



**d**



**e**



HA14-1 $\mu\text{M}$	-	5	10	20	0	5	10	20
Embelin $\mu\text{M}$	-	-	-	-	20	20	20	20

Figure 4

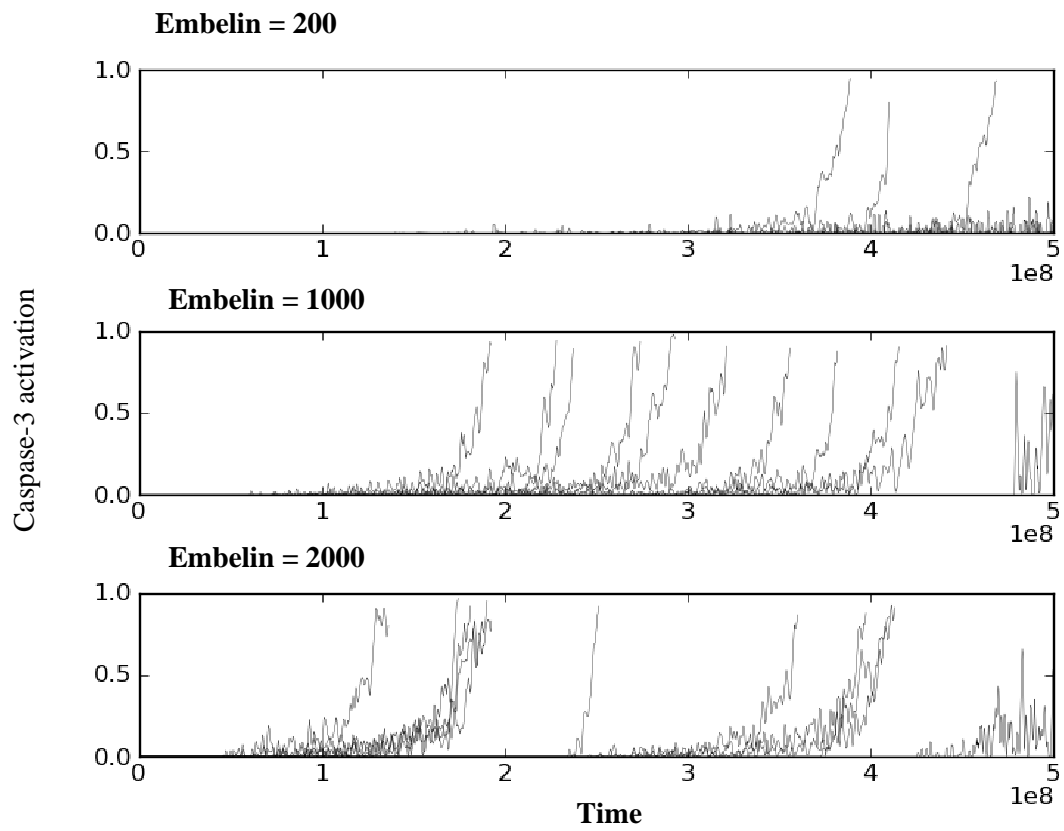
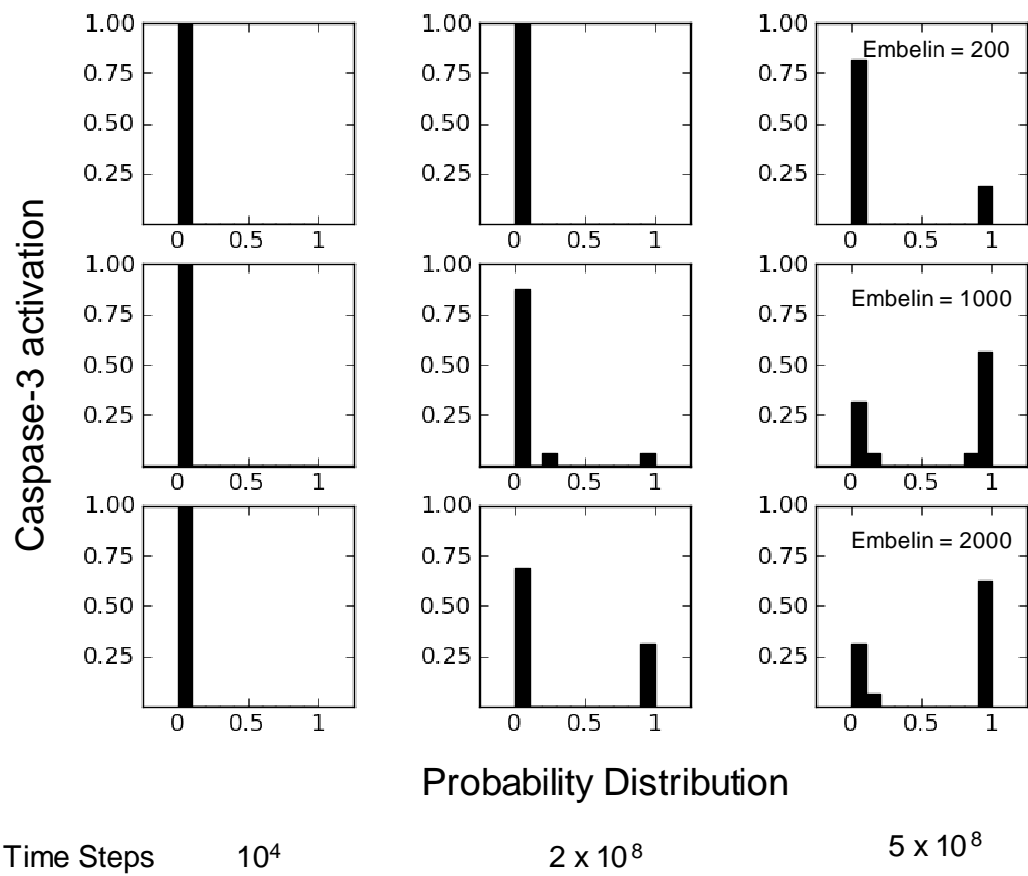
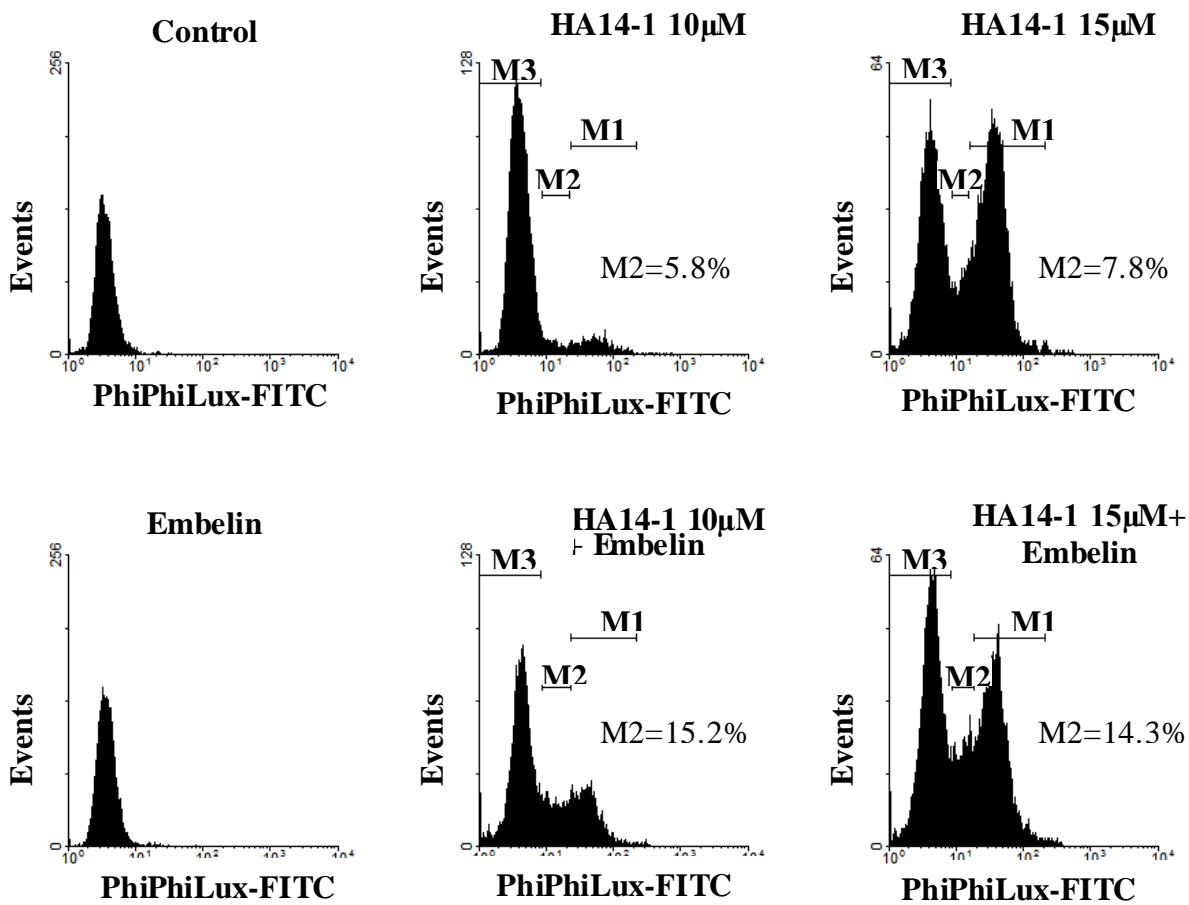


Figure 5

a.



b.



Supplementary Figure 1

